Multiplex assessment of the positions of odorant receptor-specific glomeruli in the mouse olfactory bulb by serial two-photon tomography

Bolek Zapiec[a,b] and Peter Mombaerts[a,1]

[a]Max Planck Research Unit for Neurogenetics, 60438 Frankfurt, Germany; and [b]Medical Biophysics, Institute of Physiology and Pathophysiology, Faculty of Medicine, Heidelberg University, 69120 Heidelberg, Germany

Edited by Jeremy Nathans, Johns Hopkins University, Baltimore, MD, and approved September 16, 2015 (received for review June 23, 2015)

In the mouse, axons of olfactory sensory neurons (OSNs) that express the same odorant receptor (OR) gene coalesce into one or a few glomeruli in the olfactory bulb. The positions of OR-specific glomeruli are traditionally described as stereotyped. Here, we have assessed quantitatively the positions of OR-specific glomeruli using serial two-photon tomography, an automated method for whole-organ fluorescence imaging that integrates two-photon microscopy with serial microtome sectioning. Our strategy is multiplexed. By repeated crossing, we generated two strains of mice with gene-targeted mutations at four or five OR loci for a total of six ORs: MOR23 (Olfr16), mOR37A (Olfr155), M72 (Olfr160), P2 (Olfr17), MOR256-17 (Olfr15), and MOR28 (Olfr1507). Glomerular imaging relied on intrinsic fluorescence of GFP or DsRed, or on whole-mount immunofluorescence with antibodies against GFP, DsRed, or β-gal using the method of immunolabeling-enabled three-dimensional imaging of solvent-cleared organs (iDISCO). The high-resolution 3D-reconstructed datasets were segmented to identify the labeled glomeruli and to assess glomerular positional variability between the bulbs of one mouse (intraindividual) and among the bulbs of different mice (interindividual). In 26 mice aged 21 or 50 d or 10 wk, we made measurements of the positions of 352 glomeruli. We find that positional variability of glomeruli correlates with the OR: For instance, the medial MOR28 glomerular domain occupies a surface area that is an order of magnitude larger than the surface area of the medial MOR23 glomerular domain. Our results quantify the level of precision that is delivered by the mechanisms of OSN axon wiring, differentially for the various OSN populations expressing distinct OR genes.

olfaction | glomerulus | gene targeting | axon guidance | olfactory sensory neuron

In the main olfactory system of the mouse, the elementary unit of sensory input consists of a population of olfactory sensory neurons (OSNs) that express the same odorant receptor (OR) gene and that project their axons to the olfactory bulb, where they coalesce into one or a few glomeruli (1). There are ∼1,100 intact OR genes in the mouse genome (2) and ∼3,600 glomeruli in the mouse olfactory bulb (3). How can a single elementary unit be visualized selectively among these massive numbers of OR genes and glomeruli? A genetic strategy (4) is the classical method to visualize simultaneously the cell bodies and dendrites of OSNs expressing a given OR gene at the level of the main olfactory epithelium and their axons coalescing into glomeruli at the level of the main olfactory bulb. By gene targeting in ES cells, a mutation is generated in the mouse germ line such that an OR coding sequence is coexpressed with an axonal reporter by virtue of bicistronic translation afforded by an internal ribosome entry site (IRES). Using this genetic strategy, it is also well established that the expressed OR is intimately involved in the mechanisms of axonal coalescence and in determining approximately where in the olfactory bulb these glomeruli are formed: For instance, replacement of the coding sequence of an OR by the coding sequence of another OR typically results in a shift in glomerular position (4–9).

OR-specific glomeruli form in highly restricted domains of the olfactory bulb (10–12). Glomerular positions have been characterized in the literature with a variety of adjectives, such as "stereotyped," "constant," "topographically fixed," "topographically defined," "topographically stereotypical," "stereotypically positioned," "with precise stereotypy," "invariant," "spatially invariant," "precise," "nearly identical," etc. Exactly how precise are these precise positions? The notion of stereotyped glomerular positions has been insufficiently tested, presumably because of the lack of methods for 3D anatomical reconstructions of the olfactory bulb in which the positions of OR-specific glomeruli can be determined accurately and quantitatively. Ideally, these anatomical analyses would be multiplexed, covering more than one type of OR-specific glomeruli in the same mouse.

Serial two-photon tomography is an automated method for whole-organ fluorescence imaging that integrates two-photon microscopy with serial sectioning by a built-in vibrating blade microtome (13). A process of mechanical and optical sectioning is repeated serially in an automated and fully unsupervised manner until the entire sample has been cut and imaged. The resulting images are processed automatically, producing 3D datasets that are free of the typical distortions when serial sections are imaged post hoc and the images of the individual tissue sections are aligned and reconstructed in three dimensions. Serial two-photon tomography has enabled the construction of the first mesoscale connectome of the mouse brain, based on stereotaxic injection of fluorescent tracers (14), and is rapidly emerging as a preferred method for neuroanatomical studies of mice.

Significance

In the mouse, olfactory sensory neurons choose one of ∼1,100 odorant receptor genes for expression. The receptor determines not only to what odorants the neuron responds but also in which glomerulus of the olfactory bulb its axon terminates. The positions of the ∼3,600 glomeruli are traditionally described as stereotyped. Using an automated method that cuts sections off brain samples and fluorescently images the block face, we quantitatively assess the positions for six types of glomeruli. The level of variability is more substantial than typically acknowledged, and some types of glomeruli are more variable in their position than others. Our results quantify the level of precision that is delivered by the mechanisms of axon wiring in the mouse olfactory system.

Author contributions: B.Z. and P.M. designed research; B.Z. performed research; B.Z. and P.M. analyzed data; and B.Z. and P.M. wrote the paper.

The authors declare no conflict of interest.

This article is a PNAS Direct Submission.

Freely available online through the PNAS open access option.

[1]To whom correspondence should be addressed. Email: peter.mombaerts@gen.mpg.de.

This article contains supporting information online at www.pnas.org/lookup/suppl/doi:10.1073/pnas.1512135112/-/DCSupplemental.

Here, we have applied serial two-photon tomography to the olfactory bulbs of mice that carry gene-targeted mutations of the OR-IRES design at one, four, or five OR loci. We have assessed quantitatively the positional variability of a total of six types of OR-specific glomeruli: MOR23 (Olfr16), mOR37A (Olfr155), M72 (Olfr160), P2 (Olfr17), MOR256-17 (Olfr15), and MOR28 (Olfr1507). The objective of multiplexing was achieved by repeatedly crossing gene-targeted mouse strains carrying a single tagged OR gene (4, 7, 15–19) until mice were obtained with mutations at four (4OR) or five (5OR) loci. These OR genes reside on different chromosomes, facilitating the generation of quadruple and quintuple mutant mice without the need for meiotic crossovers. The ages of the 26 mice analyzed were 21 d, 50 d, and 10 wk. We document quantitatively the level of positional variability for a total of 352 glomeruli. Our main finding is that this positional variability correlates with the OR. The MOR23 glomeruli have the least variable glomerular positions, particularly the medial MOR23 glomeruli. Multiple lines of evidence indicate that the MOR28 glomeruli have the highest positional variability. Our results quantify the level of precision that is delivered by the mechanisms of OSN axon wiring in the mouse. This level of precision appears to vary among the various OSN populations expressing distinct OR genes.

Results

Imaging Glomeruli. We quantified the level of positional variability of OR-specific glomeruli by performing measurements in mouse olfactory bulbs containing fluorescently tagged glomeruli that correspond to a particular OR. We generated high-resolution 3D datasets of bulbs using a commercially available setup for serial two-photon tomography, a method for serially capturing fluorescent images of a complete undamaged brain (13). Briefly, the TissueCyte 1000 platform (TissueVision) (Fig. 1*A*) consists of a two-photon microscope mounted over a motorized *xyz* stage with an integrated vibrating microtome. Multiple optical sections are imaged of a field of view under a 1.0-N.A. objective at a magnification of 20× mounted to a z-piezo, using a Mai Tai DeepSee Ti:Sapphire laser (Spectra-Physics) and three photomultiplier tubes. Below the objective, a brain sample embedded in an agarose block is mounted to the stage, which successively moves the sample in *x*–*y* coordinates to generate a series of overlapping image tiles that comprise a plane below the surface of the brain-agarose block. Once the superficial segment of the sample (the block face) has been imaged, the vibrating microtome cuts off and discards the imaged tissue segment in a coronal fashion. The stage then raises the sample in the *z* axis, allowing the next set of tiles to be imaged. This procedure of mechanical and optical sectioning is repeated serially in a fully

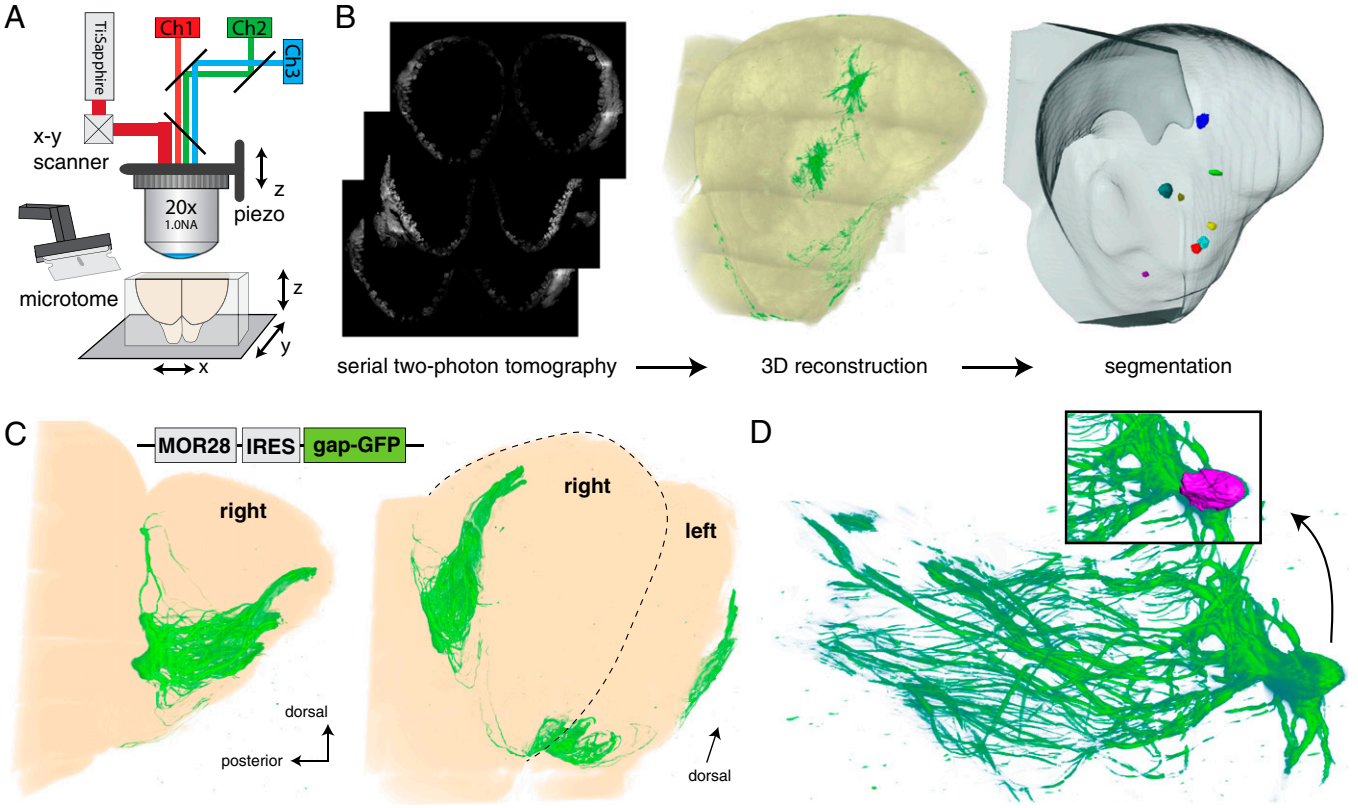

Fig. 1. Schematic of serial two-photon tomography and 3D reconstruction. (*A*) Scheme of serial two-photon tomography with the commercial TissueCyte 1000 platform. A mouse brain (or part thereof) embedded within an agarose block is attached to an *xyz* stage below an objective in a two-photon microscope that is equipped with a Ti:Sapphire laser; dichroic mirrors for channel separation; and three photomultiplier tubes corresponding to red, green, and blue channels. A z-piezo enables optical sectioning while the stage moves the sample among fields of views for imaging. An integrated vibrating blade microtome cuts off mechanical coronal sections from the top of the block serially between rounds of imaging, removing and discarding the tissue that has already been imaged. (*B*) The experimental design consists of fluorescently labeled mouse olfactory bulbs imaged using serial two-photon tomography, followed by 3D reconstruction and segmentation. This example is from an OMP-GFP mouse, in which all mature OSNs, including their axons, express GFP along with olfactory marker protein (OMP) (36). (*C*) Three-dimensional reconstruction of both olfactory bulbs of an individual mouse homozygous for the gene-targeted MOR28-IRES-gap-GFP mutation at PD21. MOR28-expressing OSNs, their axons, and their glomeruli can be visualized readily by the intrinsic fluorescence of GFP. (*D*) Magnification of axons of MOR28-expressing OSNs coalescing into glomeruli. The glomeruli were segmented into objects on the basis of the fluorescent signal from axons and are pseudocolored in purple.

unsupervised manner until the entire sample has been cut and imaged. After imaging the region of the brain that is of interest, the tiles are stitched using commercially available software, producing a stack of images, one image per channel and per optical section (Fig. 1*B* and Fig. S1). A typical image stack of the bulbs consists of ∼800 optical sections. We then reconstructed these stacks in three dimensions and segmented the objects of interest to enable direct visualization of OR-specific glomeruli (Fig. 1*B*).

MOR28 Interglomerular Distances. The MOR28 glomeruli as visualized in the MOR28-IRES-gap-GFP mouse strain constitute a popular model for studies of OSN axon wiring (18–24). In a first set of experiments, we imaged six bulbs of three littermates at postnatal day (PD) 21 that are homozygous for the gene-targeted mutation MOR28-IRES-gap-GFP (18, 19). In the gap-GFP marker, the 20 N-terminal amino acid residues of GAP43 are fused to the N terminus of GFP to target GFP to the plasma membrane (25). The 3D reconstructions show robust expression of the gap-GFP marker in axons traversing the olfactory bulb and coalescing into glomeruli in the ventral bulb (Fig. 1*C*). To determine the MOR28 glomerular positions in this mouse strain precisely, glomeruli were segmented using the fluorescent signal to designate voxels corresponding to each glomerulus (Fig. 1*D*).

The textbook case of OR-specific glomeruli in the mouse olfactory bulb is a situation of exactly two glomeruli per bulb: one glomerulus in each of the medial and lateral halves of the left and right bulbs, and thus four glomeruli per mouse. This ideal scenario is not always the case, however. Axon bundles often diverge and coalesce into two or sometimes three distinct glomeruli instead of a single glomerulus (Fig. 2*A*, blue arrows compared with orange arrow for a single glomerulus). In some bulbs of MOR28-IRES-gap-GFP mice, further divergence is seen by a small subset of axons that project still further from the region of convergence and form what appear to be microglomeruli (26); these structures are outside the scope of this study (Fig. 2*A*, red arrow, and Fig. S2*A*). For many analyses, such as measuring interglomerular distances within a bulb, these cases of two or three glomeruli interfere with the measurements because there is more than a single object per half-bulb to consider. These cases of multiple glomeruli are too common to discard as outliers, and they are not transient phenomena at PD21 but persist at PD50 and at 10 and 18 wk in the conditions of our animal facility. Because measuring twice or thrice would overrepresent half-bulbs with multiple glomeruli in any statistics, we opted to define centroids in the cases of multiple glomeruli (Fig. 2*B*). A centroid is a simple and unbiased method for defining the central location of multiple objects as the 3D midpoint. Unless otherwise noted, all our analyses used centroids for cases of multiple glomeruli in a half-bulb. One such analysis is the measurement of the interglomerular distance between the medial and lateral OR-specific glomeruli in one bulb, yielding an absolute distance in millimeters (Fig. 2*C*).

Because differences in genetic background and environmental influences, such as olfactory experience, could affect glomerular positioning, we asked whether the interglomerular distance for pairs of MOR28 glomeruli (or centroids) is similarly divergent between the left and right bulbs of the same mouse (intraindividual) compared with bulbs of different mice (interindividual). We measured interglomerular distances between pairs of MOR28 glomeruli (or centroids) of one bulb in three dimensions via straight lines through each of the six bulbs of the three mice in this first set of experiments, yielding six values (2.5 mm ± 108 μm) (Fig. 2*D*). We then calculated the deviation Δ of the interglomerular distance between a bulb and the other bulb of the same mouse [intraindividual, left and right bulbs ("L/R"), three values: 1L vs. 1R, 2L vs. 2R, and 3L vs. 3R] or between a bulb and every other bulb of the two other mice (interindividual, "all," 12 values: 1L vs. 2L, 1L vs. 2R, 1L vs. 3L, 1L vs. 3R, 1R vs. 2L, 1R vs. 2R, 1R vs. 3L, 1R vs. 3R, 2L vs. 3L, 2L vs. 3R, 2R vs. 3L, and 2R vs. 3R) (Fig. 2*E*, error bars at SD). We find that the mean and the distribution of values are comparable for intraindividual (L/R) and interindividual (all) measurements: 292 ± 241.5 μm for L/R and 316.9 ± 217.6 μm for all. Thus, the variability of MOR28 glomerular positions between the left and right bulbs of the same mouse is similar to the variability among the three littermates.

MOR28 Glomerular Positions in a Merged-Bulb Model. To expand on the comparison of interglomerular distances between bulbs of the same mice and among bulbs of different mice, we aligned the 3D reconstructions of the six individual bulbs and generated a single merged bulb (Fig. 2*F*). The left bulb was mirrored (reflected) to allow all bulbs to be aligned together as a single merged "right" bulb, which is typically depicted in the literature. The contour of the glomerular layer was used to generate a surface of the bulb that was then used for aligning the bulbs to a reference bulb. The glomerular layer was used to define the bulb surface, because dissection can affect the extent of the olfactory nerve and olfactory nerve layer attached to the bulb, which would contribute noise when aligning the bulbs. The 3D alignment of bulb surfaces was automated using a commercially available, iterative, closest point algorithm integrated in Amira (FEI) that was only allowed to pan and rotate a bulb in pursuit of a best fit. Importantly, no resizing or warping was applied, and the positions of the labeled glomeruli were not used in these alignments. We find that the alignment is robust and enables a direct 3D comparison of the six bulbs from the three homozygous MOR28-IRES-gap-GFP littermates at PD21 in this first set of experiments (Fig. 2*G* and Fig. S2*B*). We measured the size of the medial and lateral domains occupied by the MOR28 glomeruli (Fig. 2*H*). The medial MOR28 glomerular domain at PD21 spans an area of at least 0.4 mm dorsoventral by at least 0.5 mm anterior-posterior. The lateral MOR28 glomerular domain has a dorsoventral extent of at least 1.4 mm and an anterior-posterior extent of at least 0.4 mm. Some microglomerular structures (26) were present and are pictured (Fig. 2 *A*, *G*, *I*, and *H*), but they were not included in this study.

We extended the merged-bulb model in a second set of experiments, which consists of eight bulbs from four homozygous MOR28-IRES-gap-GFP littermates at a later age, PD50 (Fig. 2*I*). Again, we observe a broad spread of the MOR28 glomeruli and the occasional occurrence of microglomeruli. The medial MOR28 glomerular domain spans at least 0.6 mm dorsoventral by at least 0.4 mm anterior-posterior, and the lateral domain spans at least 2 mm dorsoventral by at least 0.5 mm dorsoventral (Fig. 2*J*).

The extensive size of the medial and lateral MOR28 glomerular domains at PD21 and PD50 complements our observations of the substantial positional variability of MOR28 glomeruli in terms of interglomerular distances. We conclude from the first and second sets of experiments that the large variance in interglomerular distances for MOR28 in the MOR28-IRES-gap-GFP mouse strain is not due to variations in overall bulb size or shape, but is primarily the result of the high level of freedom that MOR28 glomeruli appear to have in their positions in the olfactory bulb.

OR-Correlated Deviation in Glomerular Positions. We next asked if the high level of positional variability of MOR28 glomeruli is also the case for other OR-specific glomeruli. We generated a 4OR mouse strain to visualize the glomerular positions for multiple ORs in a single mouse. This multiplex strategy enables comparisons of positional variability without the influence of confounding factors, such as interindividual differences in genetic background and odor experience. The 4OR cross contains three gene-targeted mutations encoding fluorescent proteins (MOR28-IRES-gap-GFP, MOR256-17-IRES-tauGFP, and M72-IRES-tauRFP2), permitting intrinsic fluorescence imaging of the olfactory bulbs with the TissueCyte 1000 platform. The glomeruli

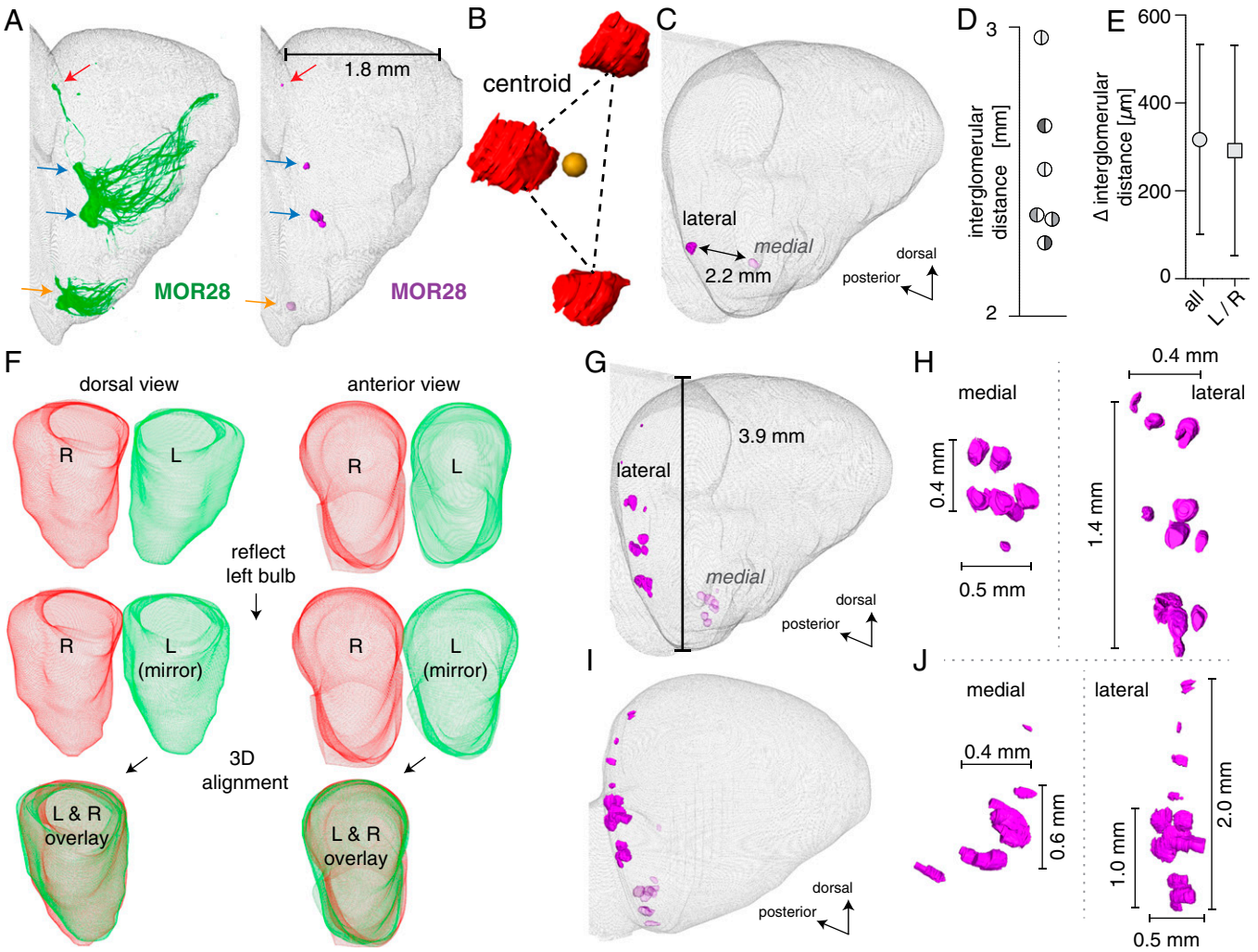

Fig. 2. Quantifying positional variability of MOR28 glomeruli at PD21 and PD50. (*A*) Three-dimensonal reconstruction of the right bulb of a PD21 MOR28-IRES-gap-GFP mouse shows axons coalescing into one glomerulus on the distal medial face (orange arrow); two glomeruli on the proximal lateral face (blue arrows); and a third structure, which appears to be a microglomerulus (red arrow). (*B*) When a half-bulb contains two or three glomeruli, the centroid was used whenever a single position was needed for calculations. Centroids are generated by computing the average position of multiple glomeruli. (*C*) Linear paths straight through the olfactory bulb between medial-lateral glomerular pairs define the interglomerular distance, which is 2.2 mm in this example. (*D*) Interglomerular distances between MOR28 medial-lateral glomerular pairs (or centroids) are plotted for the six bulbs of three MOR28-IRES-gap-GFP littermates at PD21. The three shades of gray correspond to the three mice. The filled side of the circle represents the left or right bulb. (*E*) Interglomerular distances between pairs of MOR28 glomeruli were determined for six bulbs of the three mice and compared in a pairwise fashion. The word "all" corresponds to interindividual comparisons such that each pair of bulbs tested corresponds to two mice, either left vs. left, right vs. left, or right vs. right (12 values). The L/R set is composed of intraindividual comparisons between the left and right bulbs of the same mouse (three values). (*F*) Left and right bulbs from the three homozygous MOR28-IRES-gap-GFP mice were aligned and mapped to a merged right bulb. Mirror images of the left bulbs were used to facilitate superimposition. Following iterative, rigid alignment of the bulb surface, high-quality alignment was achieved for all samples. (*G*) Alignment of the bulbs facilitates visualization of glomerular positions and assessment of their positional variability. (*H*) The medial and lateral domains of MOR28 glomeruli are spread over a large area at PD21. (*I*) Alignment of the eight bulbs of four MOR28-IRES-gap-GFP mice at PD50. (*J*) Spread of MOR28 glomeruli at PD50 is comparable to PD21.

corresponding to the P2-IRES-tau-lacZ mutation were not imaged in these experiments with 4OR mice. This third set of experiments consists of three 4OR mice at PD21, two of which were littermates. We aligned the five bulbs in a single merged right bulb (Fig. 3*A* and Fig. S3); one bulb was damaged and not further used. Next, we measured the interglomerular distances for glomerular pairs (or centroids) within a bulb for the three types of fluorescent glomeruli in the 4OR strain: MOR28, MOR256-17, and M72 (Fig. 3*B*, *Left*; error bars at SEM). The interglomerular distances for MOR28 in the 4OR strain (2.5 mm ± 108.6 μm) are nearly identical to the interglomerular distances that we measured in the single-tagged MOR28-gap-GFP strain (2.5 mm ± 108.0 μm) in the first set of experiments. The average ± SEM of the interglomerular distances over the five bulbs is 2.6 mm ± 38.1 μm for MOR256-17, and it is 1.5 mm ± 54.5 μm for M72. We then compared each value for interglomerular distance with the average distance of the five values for that OR, and identify various levels of deviation Δ from the average distance among these three ORs (Fig. 3*B*, *Right*): 47.7 ± 17.7 μm for MOR256-17, 95.8 ± 26.0 μm for M72, and 134.0 ± 53.2 μm for MOR28. These differences among ORs are not simply a function of the absolute interglomerular distances, because they persist when calculating the relative deviation: MOR28 has the highest level of positional variability, with a relative deviation of ~9 ± 3% from the average interglomerular distance, compared with 3 ± 1% for MOR256-17 and 6 ± 3% for M72 (Fig. 3*C*, error bars at SEM). We conclude that some OR-specific glomeruli are more variable in their position than others.

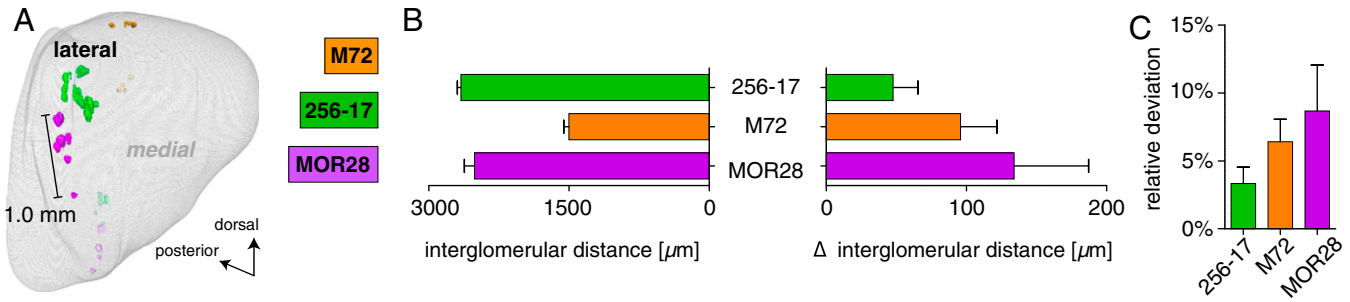

Fig. 3. Multiplex comparison of glomerular positions of MOR28, MOR256-17, and M72 at PD21. (*A*) Five bulbs from three PD21 mice of the 4OR strain, which contains three OR genes tagged with genes encoding fluorescent proteins, were reconstructed in three dimensions and aligned to a single merged right bulb, of which the lateral face is here oriented proximally. (*B*) Interglomerular distances in the five individual bulbs were determined (*Left*), and the deviation Δ of each distance from the average for that OR was calculated (*Right*) (error bars at SEM). (*C*) Differences among ORs persists even when corrected for the average absolute distance for each pair of glomeruli (error bars at SEM).

Whole-Mount Measurements Using Immunolabeling. The 4OR strain contains one OR gene tagged with tau-lacZ (a fusion of the tau with β-gal), a marker that does not afford direct imaging of intrinsic fluorescence. The P2-IRES-tau-lacZ mutation is also present in a second multiplex strain carrying gene-targeted mutations at five OR loci (5OR) that we generated in our laboratory [but it does not contain MOR28-IRES-gap-GFP, which was generated by another laboratory (18, 19)]: MOR256-17-IRES-tauGFP, P2-IRES-tau-lacZ, M72-IRES-tauRFP2, MOR23-IRES-tauGFP, and mOR37A-IRES-tauGFP. (This 5OR strain will be made publicly available from The Jackson Laboratory.) To visualize the glomeruli for a tau-lacZ–tagged OR with serial two-photon tomography, bulbs of 4OR and 5OR mice were processed using the recently reported method of immunolabeling-enabled three-dimensional imaging of solvent-cleared organs (iDISCO) for whole-mount immunofluorescence (27). We immunolabeled bulbs for GFP, β-gal, and VGLUT2 (delineating all glomeruli). The M72 glomeruli were not included in this analysis. Fluorescently labeled bulbs were imaged and reconstructed in three dimensions, and glomeruli were segmented as was done previously with intrinsic fluorescence.

This fourth set of experiments consists of 16 iDISCO-labeled bulbs from eight PD21 mice, of which four are 4OR littermates and four are 5OR littermates. An alignment into a single merged bulb with the five types of OR-specific glomeruli is shown in Fig. 4*A*. We first checked if the level of intraindividual variability is comparable to the level of interindividual variability, because the mice are still age-matched but not all are littermates. We focused on the P2 glomeruli, which are present in both mouse strains. We find that interindividual variability in deviation Δ from average interglomerular distance is similar to intraindividual variability [Fig. 4*B*; $n = 7$ (L/R) or $n = 84$ (all), error bars at SD], making comparisons between mice of the 4OR and 5OR strains within this fourth set of experiments possible (L/R = 74.6 ± 22.5 μm, all = 63.5 ± 45 μm).

The glomeruli of P2-IRES-tau-LacZ mice have been described as deviating often from the textbook case of two glomeruli per bulb (one glomerulus per half-bulb). They frequently coalesce into two or three smaller glomeruli in the vicinity of where some mice only have a single glomerulus, which is also larger (28–30). We refer to cases of a single P2 glomerulus in a half-bulb as "monoglomerular." To assess positional variability of P2 glomeruli, we averaged the monoglomerular positions of medial or lateral P2 glomeruli and calculated the distance from each glomerulus of a case of multiple glomeruli to the average monoglomerular position (Fig. 4*C*; $n = 31$, $n = 14$, $n = 14$, or $n = 27$ glomeruli or their centroids; left to right; error bars at SEM). We also measured this distance to the average monoglomerular position for centroids in cases of multiple P2 glomeruli. We find a significantly smaller deviation of the centroids from the average monoglomerular P2 position, supporting the notion that the centroids are an accurate representation of the P2 glomerular position in a particular mouse. The interglomerular distance for MOR28 and MOR256-17 remains in the range of 2–3 mm, whereas P2 and MOR23 have distances between 1.5 and 2 mm, similar to M72 (Fig. 4*D*, *Left*; MOR28 = 2.4 ± 0.06 mm, MOR256-17 = 2.8 ± 0.03 mm, P2 = 1.6 ± 0.02 mm, MOR23 = 1.9 ± 0.02 mm). We calculated the deviation Δ of each value for interglomerular distance from its average. We observe OR-correlated differences, with MOR28 having significantly more variability than P2 and MOR23 (Fig. 4*D*, *Right*; $n = 8$–14 bulbs, error bar at SEM; MOR28 = 126 ± 33 μm, MOR256-17 = 79 ± 19 μm, P2 = 45 ± 9 μm, MOR23 = 41 ± 16 μm).

Comparing interglomerular distances assesses spacing straight through the bulb between the medial and lateral domains, rather than positions within a medial or lateral glomerular domain. Therefore, we determined the average position of each type of OR-specific glomerulus in either the medial domain or the lateral domain of the single merged bulb generated from the 16 bulbs of 4OR and 5OR mice at PD21. We did so by averaging the positions of all glomeruli for that OR in that domain in the merged bulb. Because the positional averaging procedure relies on merging left and right bulbs together, we first examined the glomerular domains of all five ORs and found no obvious difference between the left and right bulbs (Fig. S4*A*). Second, we calculated the deviation Δ of the interglomerular distances in the medial or lateral glomerular domain in only left or only right bulbs (Fig. S4*B*). We find no significant difference between the average Δ values when comparing the medial domain of the left bulb with the medial domain of the right bulb or comparing the lateral domain of the left bulb with the lateral domain of the right bulb, for all five ORs. Thus, there is no asymmetry in variability between left and right bulbs. Third, we evaluated how measurements using the average position for a type of OR-specific glomerulus compare with measurements restricted to the left and right bulbs of an individual (Fig. S4*C1*). The average glomerular position (medial or lateral) for a given OR was used to measure interglomerular distances with each of the glomeruli for that OR in the other half-bulb (Fig. S4 *C2* and *C3*). We find that the average Δ values for interglomerular distances that use the average glomerular position (medial vs. average, lateral vs. average) are lower than the average Δ values for interglomerular distances in a single mouse (L/R) (Fig. S4*C4*). We performed a final test of the quality of the alignment by plotting the deviation Δ from average glomerular position values vs. the deviation Δ from average interglomerular distance values for four ORs (Fig. S4*D*). Because the interglomerular distance measurements are alignment-independent and are done in one bulb at a time, the observed coefficient of

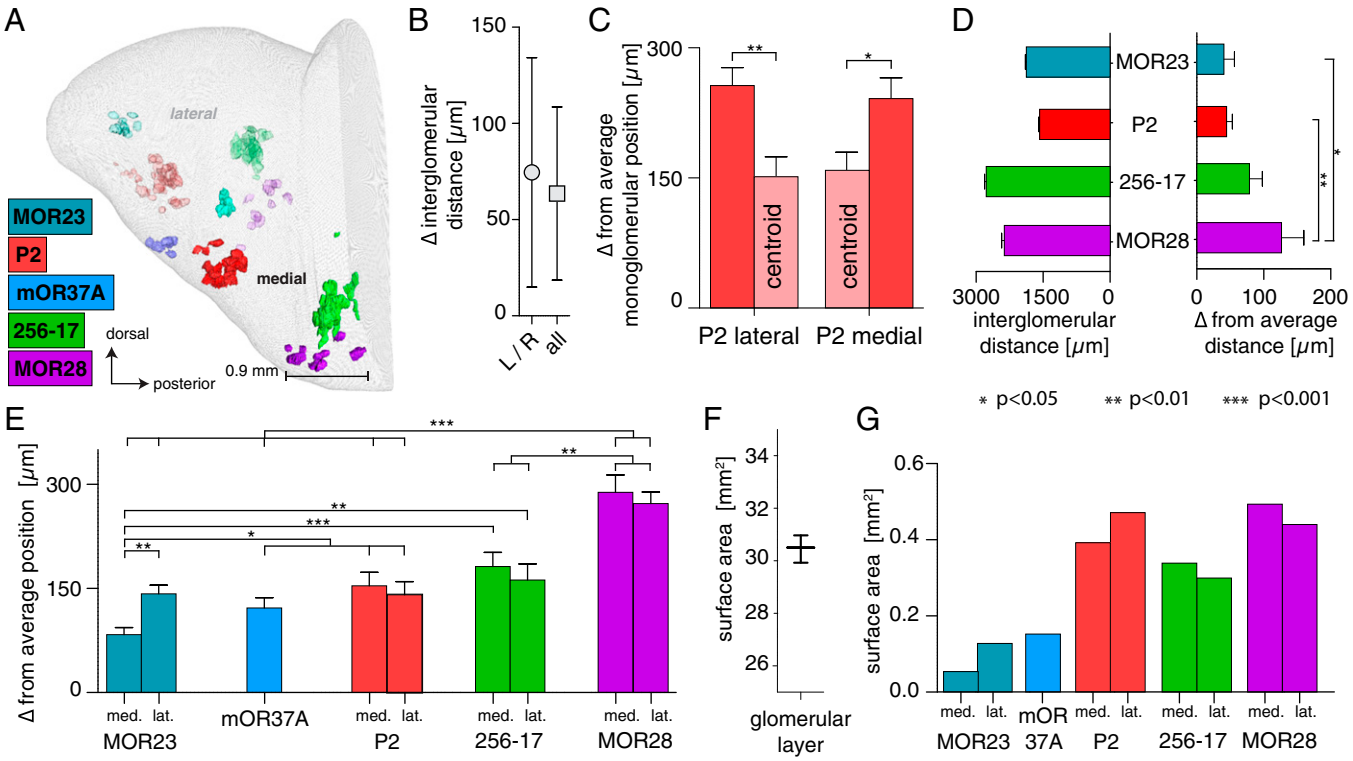

Fig. 4. Positional variability of glomeruli correlates with the OR at PD21. (*A*) Single merged right bulb, of which the medial face is shown proximally, was generated by aligning 16 bulbs from eight mice (four 4OR mice and four 5OR mice) at PD21, revealing labeled glomeruli of five ORs. Glomeruli in the distal lateral domains are shown in faded colors. (*B*) Comparison of the variability in interglomerular distance between sets of P2 glomeruli. The pairwise deviation Δ for glomerular pairs was performed on pairs consisting either of left vs. right bulbs of the same mouse (L/R) or bulbs only from two different mice: left vs. left, right vs. left, or right vs. right (all) (n = 7 or 84 values, error bars at SD). (*C*) Centroid of P2 glomeruli was evaluated by comparing its position with P2 domains that only have a single glomerulus. This average monoglomerular position was used to measure the deviation of individual multiple glomeruli, or their centroid. The deviation from the average position for these four groups is plotted and indicates that the centroid of multiple glomeruli is significantly closer to the centroid of the monoglomerular position than to its constituent glomeruli (n = 31, n = 14, n = 14, or n = 27 glomeruli or their centroids; left to right; error bars at SEM). (*D*) Interglomerular distance for glomerular pairs was determined for four ORs, and the deviation Δ for each pair from the average of that OR was calculated. MOR23 and P2 glomeruli show significantly less positional variability than MOR28 (n = 8–14, error bars at SEM). (*E*) Graph depicting the deviation Δ from the average position of that glomerulus in the merged bulb (n = 9–34 values, error bars at SEM). *(F)* Using VGLUT2 staining to detect all ~3,600 glomeruli of the main olfactory bulb, the surface area of the glomerular layer of the olfactory bulb was measured (n = 3 bulbs at PD21). (*G*) Surface area of each glomerular domain at PD21 is shown in the form of a bar graph. lat., lateral; med., medial.

determination of >0.95 provides strong validation of our concept and its execution. From this set of analyses shown in Fig. S4, we conclude that the quality of the alignment is excellent and that the average glomerular position is a valuable concept for assessing positional variability of a given type of OR-specific glomerulus within a given domain among mice. Specifically, the average glomerular position uncouples the assessment of positional variability from the need to pair glomeruli in the medial and lateral half-bulbs, which is done for calculating the interglomerular distance. Instead, positional variability can be evaluated within the medial or lateral domain separately, and can also be assessed for mOR37A glomeruli, which occupy a singular domain in the bulb.

Having thus established the robustness of the method for defining the average glomerular position, we then determined the deviation Δ for each glomerulus (or centroid) from the average glomerular position for that OR in that domain, within the single merged bulb (Fig. 4*E*; n = 8–15 half-bulbs, error bars at SEM). The measurements of deviation Δ confirm and extend that some glomeruli are more variable in their position than others. The positions of the medial MOR23 glomeruli are significantly less variable (average deviation Δ of 84 μm) than all other glomeruli in this dataset, including the lateral MOR23 glomeruli (average deviation Δ of 142 μm). Both the medial (average deviation Δ of 288 μm) and lateral (average deviation Δ of 273 μm) MOR28 glomeruli are significantly more variable in their position than all other glomeruli assessed, supporting the conclusion from the interglomerular distance measurements, which do not rely on a merged-bulb approach.

Although the pseudostratification of the olfactory bulb does offer a small degree of freedom for the lamina of the glomerular layer in which a given glomerulus is formed, the position of a glomerulus is typically confined to the surface of the bulb. We examined this property by first defining the extent of the olfactory bulb by using VGLUT2 immunolabeling to visualize all ~3,600 glomeruli in a bulb (3). We mapped out the surface of the glomerular layer and quantified its surface area as 30.47 ± 0.3 mm^2 (Fig. 4*F*). Next, we determined the surface area of the nine glomerular domains for the five ORs (Fig. 4*G*) by mapping them out on the single merged bulb with superimposed segmented glomeruli. (Note that mOR37A glomeruli occur in only one domain, which is situated approximately along the midline of the bulb.) This surface area corresponds to the region in which an OR-specific glomerulus can be found in the single merged bulb. We modeled the surface area of individual domains on an ellipse, with a minor axis and a major axis defining its extent, and performed this measurement on all glomerular domains in our dataset. Assuming that half of the total bulb surface area is medial and the other half is lateral, the relative area available to each glomerular domain is double the actual percentage of total bulb surface (except for mOR37), as follows: medial: MOR23 = 0.36%,

mOR37A = 0.5%, P2 = 3.1%, MOR256-17 = 1.96%, and MOR28 = 2.9%; lateral: MOR23 = 0.84%, P2 = 2.58%, MOR256-17 = 2.22%, and MOR28 = 3.24%. Our measurements of surface area are consistent with differences among ORs when assessing deviations in interglomerular distance (Figs. 3*B* and 4*D*) or absolute position (Fig. 4*E*). The MOR23 glomerular domains have the smallest deviation and smallest surface area, and the MOR28 glomerular domains have the largest deviation and largest surface area. For P2 and MOR256-17, the surface area results are divergent from average interglomerular distances or average deviations; the reason is that the larger surface area is due to the spread of the multiple glomeruli. This fourth set of experiments on 4OR and 5OR mice using iDISCO labeling confirms and extends the conclusion from the second and third sets of experiments: Some OR-specific glomeruli vary more in their position than others.

Positional Variability of OR-Specific Glomeruli at 10 Weeks. In a fifth and last set of experiments, we applied the iDISCO protocol to four littermates of the 4OR strain and four littermates of the 5OR strain at 10 wk, totaling 16 bulbs. Having identified in the meantime an iDISCO-compatible antibody for DsRed, these experiments also include the M72 glomeruli, which we had omitted from the fourth set of experiments at PD21. Aligning bulbs from these eight mice required an adjustment to the 3D registration parameters because the bulbs from the 5OR strain are ∼5% larger than the bulbs from the 4OR mice at this age; we used uniform shrinking to enable a comparison of the bulbs of these two types of mice. Examination of the single merged 10-wk-old bulb reveals a similar distribution and dispersion of glomeruli as observed at PD21 (Fig. 5*A*). Measuring the deviation Δ from the average glomerular position (Fig. 5*B*) confirms that glomeruli in the medial and lateral MOR28 glomerular domains show a significantly higher level of positional variability compared with all other domains analyzed. The positions of the medial MOR23 glomeruli continue to the least variable. We found a similar incidence of multiple glomeruli in all domains at PD50, 10 and 18 wk vs. PD21 (Fig. S5). Interestingly, a direct comparison of the average deviation Δ from the average glomerular position for all nine glomerular domains suggests remarkably stable levels of positional deviation, without significant difference between these two age groups (Fig. 5*C*). We conclude from this fifth set of experiments that the olfactory bulb of PD21 mice presents an accurate model for assessing glomerular positions of these six

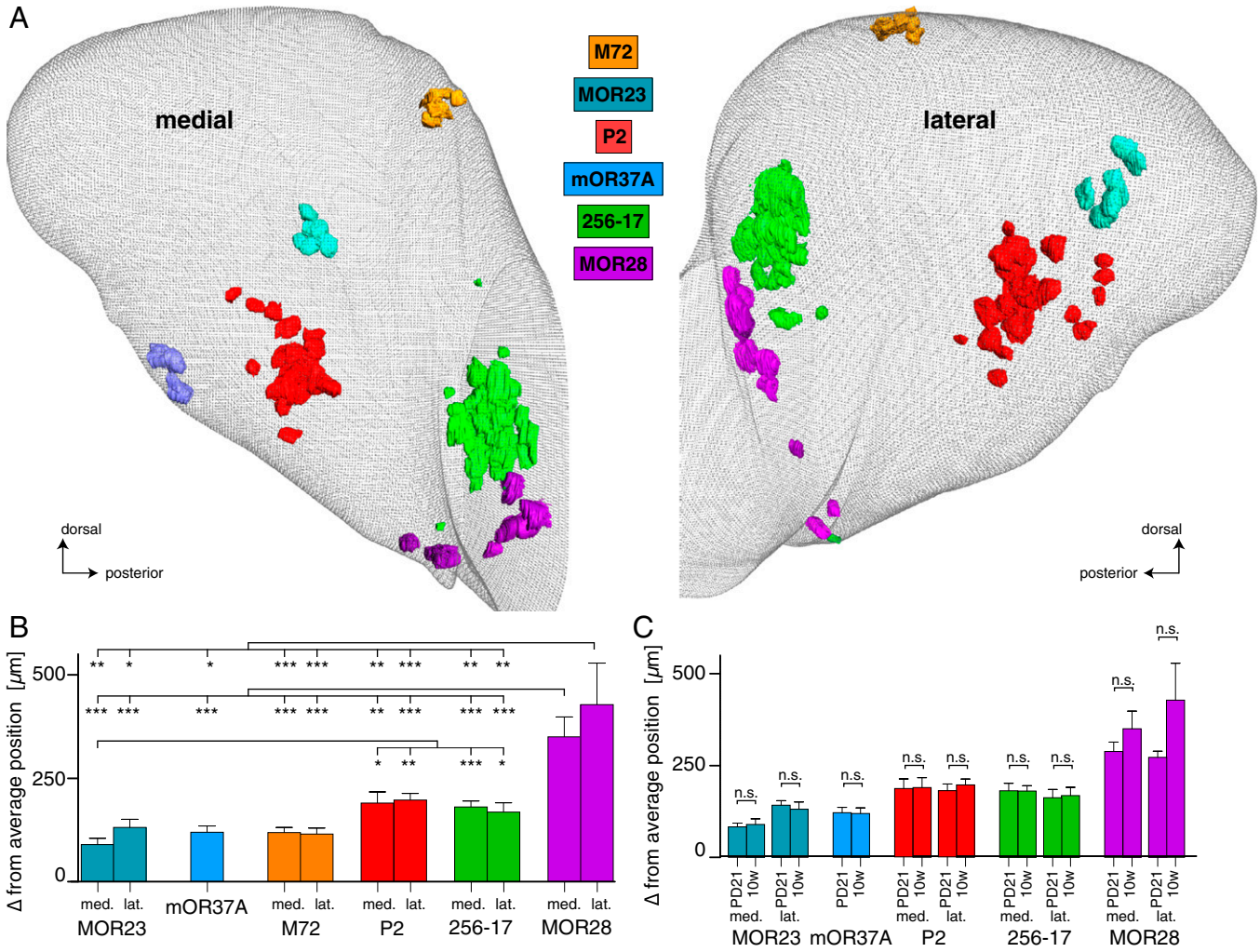

Fig. 5. Positional variability correlates with the OR at 10 wk. (*A*) Merged "right bulb" showing glomeruli from 16 bulbs of eight 10-wk-old mice (four 4OR mice and four 5OR mice) revealing labeled glomeruli of six ORs. Views of the medial surface (*Left*) and the lateral surface (*Right*) are shown. (*B*) Graph depicting the deviation Δ from the average glomerular position in the merged bulb (n = 6–16 glomeruli, error bars at SEM). (*C*) There is no significant difference in the deviation Δ from the average glomerular position between mice at PD21 vs. 10 wk. *$P < 0.05$; **$P < 0.01$; ***$P < 0.001$; n.s., not significant.

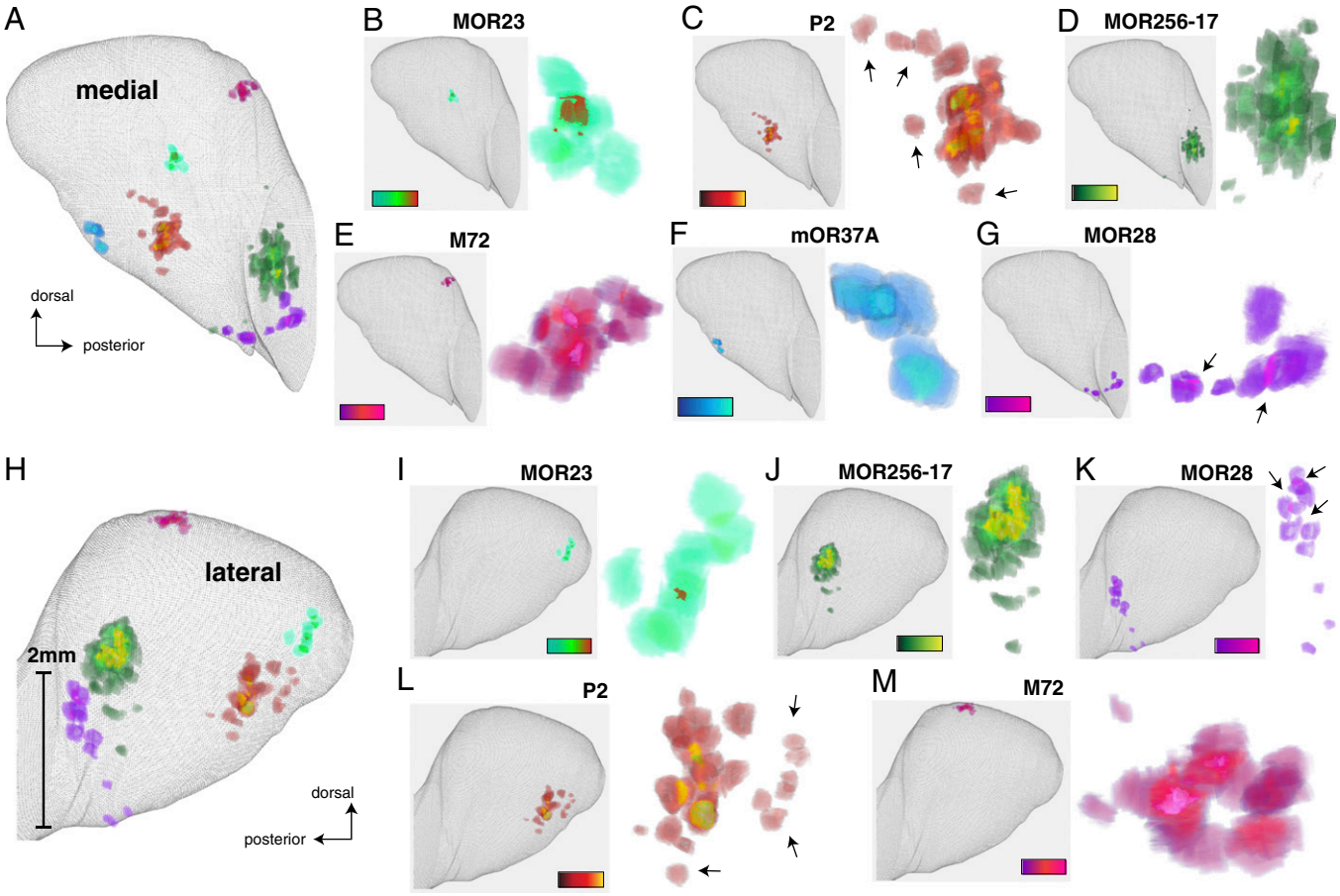

Fig. 6. Heat map rendering of frequency density for OR-specific glomeruli in three dimensions at 10 wk. (*A–K*) Three-dimensional rendering of the merged bulb with labeled glomeruli from four 4OR mice and four 5OR mice at 10 wk. The frequency of overlap for glomeruli of a given type is encoded in a color gradient representing regions of more frequent location. (*A*) Medial view, including the medial domains of MOR23, P2, MOR256-17, M72, and MOR28, and the singular domain of mOR37A. (*B*) The medial MOR23 domain exhibits dense grouping of glomeruli and a conserved area of high overlap, shown in green and red. (*C*) The medial P2 domain is broad, particularly due to the occurrence of multiple glomeruli on the periphery as indicated by the arrows. The area of high density and high overlap is visible in yellow in the center. (*D*) The medial MOR256-17 domain is large, partly due to the large size of the glomerulus, but it still exhibits a core region of overlap, depicted in light green-yellow. (*E*) The medial M72 domain is located at the posterior-dorsal extent of the bulb and exhibits relatively tight grouping, with areas of overlap centered around a core region of the domain. (*F*) The singular mOR37A domain is tightly grouped with a region of high overlap, shown in turquoise. (*G*) The medial MOR28 domain is broad, with glomeruli scattered over a large region and with two small regions of overlap indicated by arrows (pink). (*H*) Lateral view of the merged bulb showing the lateral domains of MOR23, MOR256-17, MOR28, P2, and M72. (*I*) The lateral MOR23 domain is somewhat broader in extent compared with its medial counterpart but still shows a region of high overlap. (*J*) The lateral MOR256-17 domain exhibits comparable features to the medial MOR256-17 domain, with similar spread and conservation of the core region. (*K*) The lateral MOR28 domain is similarly broad to the medial MOR28 domain, with only slivers of overlap between glomeruli indicated with arrows (pink). (*L*) The lateral P2 domain is somewhat broader than the medial P2 domain, due to the broad area corresponding to the locations of multiple glomeruli indicated by arrows. However, the core P2 lateral domain still has a core region with overlapping glomeruli (shown in yellow). (*M*) The lateral M72 domain exhibits characteristics comparable to the medial M72 domain, with a relatively tight grouping and regions of overlap corresponding to the core region of the domain.

types of OR-specific glomeruli and that the relative levels of positional variability among ORs are conserved between PD21 and 10 wk.

All Glomerular Domains Except MOR28 Exhibit Core Regions of High Density. Having visualized the glomerular patterns of 16 superimposed bulbs from the eight 4OR or 5OR mice at PD21 (Fig. S6) and 10 wk that were merged into a single bulb in each case, we generated a heat map visualization of the frequency density of glomeruli in 3D space (Fig. 6 and Movie S1). Regions of high density for individual domains are differentiated from regions of lower density by using a pseudocolor gradient unique to each OR, enabling their visualization on the same merged bulb (Fig. 6 *A* and *H* and Fig. S6 *A* and *G*). MOR23, P2, MOR256-17, M72, and mOR37A have core regions of high overlap (Fig. 6 *B–F*, *I–K*, and *M* and Fig. S6 *B–D*, *F*, *H*, *I*, and *K*) in both the medial and lateral domains. In contrast, MOR28 glomeruli are spread over a wider area and only have tiny slivers of overlap (Fig. 6 *G* and *K* and Fig. S6 *E* and *J*, arrows.) Thus, consistent with the conclusions of the measurements of interglomerular distance (Figs. 3*B* and 4*D*), of absolute position (Fig. 4*E*), and of surface area of glomerular domains (Fig. 4*G*), the heat map data provide the fourth line of evidence that there is range of positional variabilities among the ORs studied, with MOR28 showing the highest level of positional variability.

Discussion

Assessing glomerular positions poses a formidable experimental challenge for several reasons. First, the number of glomeruli in the adult mouse olfactory bulb is massive (~3,600). Second, the shape of the bulb does not correspond to a simple geometric structure, such as a sphere or cylinder. The bulb is medial-lateral asymmetrical: The medial surface is nearly flat, and the lateral surface follows the curvature of the skull. The surface of the bulb

is irregular. The bulb has no natural or easily identifiable axes, including no obvious anterior-posterior or dorsoventral axes. Third, there are no obvious fiducial points (i.e., no landmarks). Nonetheless glomerular positions have traditionally been characterized as stereotyped, constant, topographically fixed, invariant, etc. However, even neuroanatomical methods with relatively low precision had begun early to question the proposed invariance of glomerular positions and introduced the concept of local permutations (16, 29). Functional imaging studies have also documented positional variability of the signal that corresponds to odorant-responsive glomeruli (31, 32). Our method for aligning olfactory bulbs from multiple mice into a merged bulb has advantages over traditional whole-mount microscopy: The precise curvature of the bulb is accounted for, and the measurements are independent of the inherent positional and angle-of-view effects that are detrimental to whole-mount or section-based approaches. In comparison to 2D "roll-out" mapping methods, treating the bulb as a 3D object avoids the distortions that are inherent to projections of 3D objects with complex contours onto 2D planes. Because the entire sample is imaged intact, the results are not dependent on the orientation of the sample or the cutting plane. Importantly, our method covers all ∼3,600 glomeruli of the olfactory bulb, in contrast to functional imaging, which is confined to the dorsal olfactory bulb and covers only ∼200 glomeruli (33). Finally, our method is based on commercially available imaging equipment and software. The 5OR strain will be made publicly available from The Jackson Laboratory.

Positional variability of MOR28 glomeruli is actually apparent when surveying the images and sketches that have appeared in the literature (22–24). The degree of positional variability has thus far not been quantified, however. By applying the method of serial two-photon tomography, we have revisited the notion of stereotyped glomerular positions with a state-of-the-art, precise, unbiased, and multiplexed approach. We have quantified the level of positional variability for six ORs in three mouse strains in five sets of experiments using four independent measures, totaling 352 glomeruli in 51 bulbs of 26 mice at the age of 21 or 50 d or 10 wk. The variability in interglomerular distance of MOR28 glomeruli (Fig. 4*D*) is consistent with their large deviation from the average glomerular position in both the medial and lateral domains (Figs. 4*E* and 5*B*), is complementary to the large surface area of the MOR28 glomerular domains (Fig. 4*G*), and is further illustrated by the lack of a core region in the heat map rendering (Fig. 6 *G* and *K* and Fig. S6 *E* and *J*). The large surface area of the P2 glomerular domain is due to the frequent tendency for P2 axons in this study to form multiple glomeruli in the vicinity of the monoglomerular location. However, after this tendency of P2 is corrected using the centroid model for multiple glomeruli, the deviation from the average position matches the values measured for other ORs. However, even with the centroid correction, the MOR28 glomeruli occupy a much larger domain in the bulb than the other ORs.

By using multi-OR–tagged strains, we multiplexed the analysis in a single mouse and assessed position and variability with a whole-organ approach, enabling comparison of OR-specific glomeruli without the caveats of comparing different strains each carrying a single tagged OR gene. The similarity in average deviation Δ for both the medial and lateral domains of a given OR suggests that the level of precision is a function of the OR protein itself and/or the type or population of OSNs that have chosen to express this OR. Coding sequence replacements can address the effect of the expressed OR and OSN type or population on positional variability, but because the corresponding glomeruli are typically located elsewhere in the bulb, it will be necessary to study many combinations. Specific OR antibodies combined with a whole-mount method, such as iDISCO, should enable us to determine positional variability of glomeruli in wild-type inbred mice, without possible confounding factors of genetic manipulation, marker proteins, and the mixed genetic background. It cannot be excluded that positional variability for a given OR, such as MOR28, varies from strain to strain, depending on the marker protein, the gene targeting design, or strain construction.

The differences in levels of positional variability are relevant for studies that use glomerular positions for investigating the mechanisms that underlie the coalescence of OSN axons into glomeruli. In the case of MOR28-IRES-gap-GFP, the range of deviation Δ from its average position for medial glomeruli (mean = 288 μm) and lateral glomeruli (mean = 373 μm) makes this strain less suitable for the study of the mechanisms of axonal coalescence into glomeruli. Moreover, the variability is not uniform along all axes, with the lateral MOR28 domain spanning at least 1 mm along its major axis and at least 500 μm on the minor axis at PD21. By contrast, using a glomerulus for an OR with a significantly smaller degree of positional variability, this source of potential error can be avoided, allowing the investigation of much finer positional shifts. The medial MOR23 glomerulus lends itself well to such a role, with major and minor axes of 290 μm and 237 μm, respectively, at PD21 and the lowest mean deviation Δ (84 μm) from its average glomerular position. We have also reported that the number of MOR23-expressing OSNs has the lowest interindividual variability among a set of 11 ORs for which we have generated strains of the OR-IRES design (34).

Conclusions

Our method for mapping glomerular positions in the mouse olfactory bulb is intuitive, quantitative, and reliable. It is based on commercially available imaging equipment and software and covers the entire bulb. Our approach affords high precision while accounting for factors such as the shape of the bulb and interindividual variability. We have assessed quantitatively the positional variability for six types of OR-specific glomeruli using single- and multi-OR–tagged mice at PD21, PD50, and 10 wk. Our main finding is that positional variability differs among OR-specific glomeruli, as visualized in this set of publicly available gene-targeted strains of the OR-IRES–marker design in the conventional 129 × B6 mixed background. Our results define the level of precision that is delivered by the mechanisms of OSN axonal wiring differentially for the various populations of OSNs expressing distinct ORs.

Materials and Methods

Mice. The 4OR- and 5OR-tagged mice were generated by repeatedly crossing gene-targeted mouse strains. Mice were maintained in specified pathogen-free conditions in individually ventilated cages of the Tecniplast green line. Mice received ad libitum gamma-irradiated ssniff V1124-727 (ssniff, Soest, Germany). Nesting, bedding, and enrichment were provided as nestpak, Datesand Grade 6 (Datesand, Manchester, United Kingdom). Mouse experiments were performed in accordance with the German Animal Welfare Act, European Communities Council Directive 2010/63/EU, and institutional ethical and animal welfare guidelines of the Max Planck Institute of Biophysics and the Max Planck Research Unit for Neurogenetics. Approval came from the Regierungspräsidium Darmstadt and the Veterinäramt of the City of Frankfurt. Our 5OR strain will be made publicly available from The Jackson Laboratory as JR#27730, with the official strain name STOCK Olfr16< tm2Mom> Olfr155< tm2Mom> Olfr17< tm1Mom> Olfr160< tm7Mom> Olfr15<tm2Mom>/MomJ. The MOR28-IRES-gap-GFP strain was provided by the RIKEN BioResource Center through the National BioResource Project of the Ministry of Education, Culture, Sports, Science and Technology, Japan.

Tissue Processing. Mice of both sexes at PD21, PD50, or 10 wk were anesthetized with an i.p. injection of ketamine/xylazine sodium chloride (NaCl) solution (210 mg/kg of ketamine, 10 mg/kg of xylazine). Mice were perfused with ice-cold 0.9% NaCl solution, and then with 15 mL of 4% paraformaldehyde in PBS. The olfactory bulbs were dissected and postfixed overnight at 4 °C.

Whole-Mount Immunolabeling. Samples were processed according to the iDISCO protocol (27). Primary antibodies were chicken anti-GFP (GFP-1020;

Aves Labs), chicken anti–β-gal (ab9361; Abcam), rabbit anti-RFP (039600-401-379; Rockland Immunochemicals), and guinea pig anti-VGLUT2 (135 404; Synaptic Systems). Secondary antibodies were donkey anti-chicken Rhodamine Red X (703-295-144; Jackson ImmunoResearch Laboratories), donkey anti-rabbit Alexa 488 (A21206; Invitrogen), and donkey anti-guinea pig aminomethylcoumarin acetate (AMCA) (706-155-148; Jackson ImmunoResearch Laboratories).

Serial Two-Photon Tomography. Three-dimensional, serial block-face, two-photon microscopy was performed with a TissueCyte 1000 scanner (TissueVision) equipped with a Zeiss 20× magnification/1.0 N.A. objective and a Ti:Sapphire laser (Mai Tai HP DeepSee; Spectra-Physics) tuned to 800 nm. Samples with intrinsic fluorescence or immunofluorescence were prepared as described by the manufacturer (13). Mechanical section thickness was set at 100 μm. Optical z-stacks were captured at an *x–y* resolution of 1.02 μm per pixel and 5 μm per z-plane. Stacks were captured starting 50 μm below the cutting plane until a depth of 150 μm was reached, thus spanning 100 μm in the *z* axis.

Three-Dimensional Reconstruction and Analysis. Stacks of images produced by serial two-photon tomography were processed using custom Python, MATLAB (MathWorks), and ImageJ scripts provided by TissueVision. Three-dimensional reconstruction and measurements were performed with Amira 6 (FEI). Bulb surfaces were generated by generating contours of the glomerular layer either from VGLUT2 signal or from autofluorescence in samples undergoing intrinsic fluorescence imaging. Registration of bulb surfaces was based on the AlignSurfaces module in Amira, which allows registration of surfaces by minimizing the root mean square distance between all points comprising the surface of a reference bulb and all points from the surface of the bulb being aligned (Procrustes analysis). This registration is achieved via an iterative closest point algorithm, which applies the rigid transformations in succession while attempting to minimize the root mean square distance (35). Statistical analysis (two-tailed *t* test) was performed with GraphPad Prism 5.

ACKNOWLEDGMENTS. We thank Olaf Christian Bressel and Mona Khan for the breeding and genotyping of 4OR and 5OR mice over several years and Martin Vogel for help in setting up the TissueCyte 1000 platform. P.M. thanks, in particular, Peter Gruss for support in acquisition of the TissueCyte 1000 platform, without which this study would not have been possible. P.M. was supported by the Max Planck Society and European Research Council Advanced Grant ORGENECHOICE.

1. Bozza T, Feinstein P, Zheng C, Mombaerts P (2002) Odorant receptor expression defines functional units in the mouse olfactory system. *J Neurosci* 22(8):3033–3043.
2. Buck L, Axel R (1991) A novel multigene family may encode odorant receptors: A molecular basis for odor recognition. *Cell* 65(1):175–187.
3. Richard MB, Taylor SR, Greer CA (2010) Age-induced disruption of selective olfactory bulb synaptic circuits. *Proc Natl Acad Sci USA* 107(35):15613–15618.
4. Mombaerts P, et al. (1996) Visualizing an olfactory sensory map. *Cell* 87(4):675–686.
5. Wang F, Nemes A, Mendelsohn M, Axel R (1998) Odorant receptors govern the formation of a precise topographic map. *Cell* 93(1):47–60.
6. Feinstein P, Mombaerts P (2004) A contextual model for axonal sorting into glomeruli in the mouse olfactory system. *Cell* 117(6):817–831.
7. Feinstein P, Bozza T, Rodriguez I, Vassalli A, Mombaerts P (2004) Axon guidance of mouse olfactory sensory neurons by odorant receptors and the beta2 adrenergic receptor. *Cell* 117(6):833–846.
8. Mombaerts P (2006) Axonal wiring in the mouse olfactory system. *Annu Rev Cell Dev Biol* 22:713–737.
9. Bozza T, et al. (2009) Mapping of class I and class II odorant receptors to glomerular domains by two distinct types of olfactory sensory neurons in the mouse. *Neuron* 61(2):220–233.
10. Ressler KJ, Sullivan SL, Buck LB (1994) Information coding in the olfactory system: Evidence for a stereotyped and highly organized epitope map in the olfactory bulb. *Cell* 79(7):1245–1255.
11. Axel R (2005) Scents and sensibility: A molecular logic of olfactory perception (Nobel lecture). *Angew Chem Int Ed Engl* 44(38):6110–6127.
12. Buck LB (2005) Unraveling the sense of smell (Nobel lecture). *Angew Chem Int Ed Engl* 44(38):6128–6140.
13. Ragan T, et al. (2012) Serial two-photon tomography for automated ex vivo mouse brain imaging. *Nat Methods* 9(3):255–258.
14. Oh SW, et al. (2014) A mesoscale connectome of the mouse brain. *Nature* 508(7495):207–214.
15. Vassalli A, Rothman A, Feinstein P, Zapotocky M, Mombaerts P (2002) Minigenes impart odorant receptor-specific axon guidance in the olfactory bulb. *Neuron* 35(4):681–696.
16. Strotmann J, et al. (2000) Local permutations in the glomerular array of the mouse olfactory bulb. *J Neurosci* 20(18):6927–6938.
17. Khan M, Vaes E, Mombaerts P (2011) Regulation of the probability of mouse odorant receptor gene choice. *Cell* 147(4):907–921.
18. Serizawa S, et al. (2000) Mutually exclusive expression of odorant receptor transgenes. *Nat Neurosci* 3(7):687–693.
19. Ishii T, et al. (2001) Monoallelic expression of the odourant receptor gene and axonal projection of olfactory sensory neurones. *Genes Cells* 6(1):71–78.
20. Tsuboi A, et al. (1999) Olfactory neurons expressing closely linked and homologous odorant receptor genes tend to project their axons to neighboring glomeruli on the olfactory bulb. *J Neurosci* 19(19):8409–8418.
21. Serizawa S, et al. (2003) Negative feedback regulation ensures the one receptor-one olfactory neuron rule in mouse. *Science* 302(5653):2088–2094.
22. Serizawa S, et al. (2006) A neuronal identity code for the odorant receptor-specific and activity-dependent axon sorting. *Cell* 127(5):1057–1069.
23. Takeuchi H, et al. (2010) Sequential arrival and graded secretion of Sema3F by olfactory neuron axons specify map topography at the bulb. *Cell* 141(6):1056–1067.
24. Takahashi H, Yoshihara S, Nishizumi H, Tsuboi A (2010) Neuropilin-2 is required for the proper targeting of ventral glomeruli in the mouse olfactory bulb. *Mol Cell Neurosci* 44(3):233–245.
25. Moriyoshi K, Richards LJ, Akazawa C, O'Leary DD, Nakanishi S (1996) Labeling neural cells using adenoviral gene transfer of membrane-targeted GFP. *Neuron* 16(2):255–260.
26. Lipscomb BW, Treloar HB, Greer CA (2002) Novel microglomerular structures in the olfactory bulb of mice. *J Neurosci* 22(3):766–774.
27. Renier N, et al. (2014) iDISCO: A simple, rapid method to immunolabel large tissue samples for volume imaging. *Cell* 159(4):896–910.
28. Royal SJ, Key B (1999) Development of P2 olfactory glomeruli in P2-internal ribosome entry site-tau-LacZ transgenic mice. *J Neurosci* 19(22):9856–9864.
29. Schaefer ML, Finger TE, Restrepo D (2001) Variability of position of the P2 glomerulus within a map of the mouse olfactory bulb. *J Comp Neurol* 436(3):351–362.
30. Costanzo RM, Kobayashi M (2010) Age-related changes in p2 odorant receptor mapping in the olfactory bulb. *Chem Senses* 35(5):417–426.
31. Oka Y, et al. (2006) Odorant receptor map in the mouse olfactory bulb: In vivo sensitivity and specificity of receptor-defined glomeruli. *Neuron* 52(5):857–869.
32. Soucy ER, Albeanu DF, Fantana AL, Murthy VN, Meister M (2009) Precision and diversity in an odor map on the olfactory bulb. *Nat Neurosci* 12(2):210–220.
33. Ma L, et al. (2012) Distributed representation of chemical features and tunotopic organization of glomeruli in the mouse olfactory bulb. *Proc Natl Acad Sci USA* 109(14):5481–5486.
34. Bressel OC, Khan M, Mombaerts P (2015) Linear correlation between the number of olfactory sensory neurons expressing a given mouse odorant receptor gene and the total volume of the corresponding glomeruli in the olfactory bulb. *J Comp Neurol*, 10.1002/cne.23835.
35. Besl PJ, McKay ND (1992) A method for registration of 3D shapes. *IEEE Trans Pattern Anal Mach Intell* 14(2):239–256.
36. Potter SM, et al. (2001) Structure and emergence of specific olfactory glomeruli in the mouse. *J Neurosci* 21(24):9713–9723.